STRUCTURAL AND OPTICAL STUDIES ON Ti-DOPED ZnCdO NANOCOMPOSITES FOR OPTOELECTRONIC DEVICE APPLICATION**

M. Seshu Kumar [1], P. Jayaprada [1], R. V. S. S. N. Ravikumar [2], M. C. Rao [1*]

[1] Department of Physics, Andhra Loyola College, Vijayawada, India;
e-mail: raomc72@gmail.com
[2] Department of Physics, Acharya Nagarjuna University, Nagarjuna Nagar, Guntur, India

ZnCdO is a perfect material for ZnO-based gadgets. ZnCdO nanocomposites are mainly used in most optoelectronic and display device applications. In the present investigation, a simple solution method was used to synthesize pure ZnCdO and Ti-doped ZnCdO nanocomposites with different wt% ratios (0.1, 0.3, and 0.5%). Characterization techniques such as the structural, morphological, and elemental composition of the prepared samples were undertaken by X-ray diffraction, scanning electron microscopy (SEM), energy-dispersive X-ray analysis, and photoluminescence (PL). The diffraction peaks of the prepared samples revealed the cubic phase structure. SEM showed the presence of spherical chunks with irregular grains due to agglomeration. For the prepared sample of pure ZnCdO, the particle size was found to be 62.08 nm, whereas Ti-doped ZnCdO nanocomposites (0.1, 0.3, and 0.5%) were at 55.08, 50.03, and 45.08 nm. The peak observed in PL spectra at 520 nm could be ascribed to the near-band-edge emission. The photo-generated electrons have been trapped in to Ti^{4+} levels in the forbidden gap, which enhanced the deep-level emission.

Keywords: *Ti-doped ZnCdO, X-ray diffraction, scanning electron microscopy, energy-dispersive X-ray analysis, photoluminescence.*

СТРУКТУРНЫЕ И ОПТИЧЕСКИЕ СВОЙСТВА НАНОКОМПОЗИТОВ ZnCdO, ЛЕГИРОВАННЫХ Ti, ДЛЯ ПРИМЕНЕНИЯ В ОПТОЭЛЕКТРОННЫХ УСТРОЙСТВАХ

M. Seshu Kumar [1], P. Jayaprada [1], R. V. S. S. N. Ravikumar [2], M. C. Rao [1*]

УДК 535.37;535.42/.44;620.3

[1] Колледж Андхра Лойола, Виджаявада, Индия; e-mail: raomc72@gmail.com
[2] Отделение физики Университета Ачарьи Нагарджуны, Нагарджуна Нагар, Гунтур, Индия

(Поступила 4 апреля 2022)

Для синтеза чистого ZnCdO и нанокомпозитов ZnCdO, легированных титаном с различными соотношениями (0.1, 0.3 и 0.5 мас.%), использован простой метод растворения. Структурный, морфологический и элементный анализ образцов проведен с помощью рентгеновской дифракции, сканирующей электронной микроскопии (СЭМ), энергодисперсионного рентгеновского анализа и фотолюминесценции (ФЛ). Дифрактограммы образцов выявляют кубическую фазовую структуру. С помощью СЭМ обнаружено наличие сферических образований с неправильными зернами из-за агломерации. Для образца чистого ZnCdO размер частиц 62.08 нм, для Ti (0.1, 0.3 и 0.5%)-легированных нанокомпозитов ZnCdO — 55.08, 50.03 и 45.08 нм. Максимум в спектрах ФЛ при 520 нм можно отнести к излучению вблизи края полосы. Фотогенерированные электроны захватываются на уровни Ti^{4+} в запрещенной зоне, что усиливает излучение глубоких уровней.

Ключевые слова: *легированный титаном ZnCdO, рентгеновская дифракция, сканирующая электронная микроскопия, энергодисперсионный рентгеновский анализ, фотолюминесценция.*

** Full text is published in JAS V. 90, No. 4 (http://springer.com/journal/10812) and in electronic version of ZhPS V. 90, No. 4 (http://www.elibrary.ru/title_about.asp?id=7318; sales@elibrary.ru).

Introduction. In the present scenario, researchers have mainly focused on the preparation of nanopowders by various doping materials, because these semiconducting nanopowders are at the cutting edge of nanotechnology as a result of a wide range of applications such as nano-devices, sensors, opto-luminescence, photonics, data storage devices, etc. These nanopowders possess excellent photocatalytic and antimicrobial activities owing to their surface characteristics, shape, and size. Semiconductor nanomaterials such as CdO, ZnO, and TiO_2 are used in various applications such as solar cells, flat panel displays, and photovoltaic devices, owing to their small optical bandgap within the range 2.2–2.7 eV [1]. Zinc oxide nanoparticles are used in various fields such as LEDs and solar cells owing to their special features such as wide bandgap, i.e., 3.6 eV and large excitation binding energy of 60 meV [2, 3]. They are chemically stable at room temperature. Semiconductor TiO_2 has an optical bandgap of 3.2 to 3.29 eV. It has direct and indirect transitions from 3.69 to 3.78 eV [4]. Various methods are used for the preparation of Ti-doped ZnO nanostructures such as pulsed laser deposition, chemical vapor deposition, and sputtering [5]. Among various transition metal oxides, TiO_2 is a stunning electrode material. It is used in commercial applications owing to its high specific capacitance and magnificent cycle-life stability [6]. The TiO_2 material is highly transparent in the visible region [7]. CdO nanoparticles are less toxic in nature than all other semiconductor nanoparticles [8–10]. They are used as transparent electrodes in solar cells owing to their sharp exciton transition [11–14]. The performance of the supercapacitors depends on the properties of the electrode materials. Semiconductor metal oxides are also used in optoelectronic device applications such as photo-catalyst and sensing elements [15–17].

ZnCdO is likewise viewed as a perfect material for ZnO-based gadgets. The joining of Cd into ZnO is valuable for the manufacture of $ZnO/Zn_{1-x}Cd_xO$ heterojunction and super grid, which is the key component in ZnO-based LEDs [2]. Moreover, the application of ternary ZnCdO alloys may extend the potential of ZnO-based devices further, considering that bandgap engineering is essential for fabricating heterostructures for light emitting or laser diodes, multi-junction solar cell applications, etc. Cd and Zn belong to group IIb of the periodic table and possess similar physical and chemical properties owing to similar valence electron structures. Cd-dopant in ZnO is considered one of the most promising candidates for narrowing the bandgap energy of ZnO. Such properties indicate that Cd could be incorporated into ZnO to be used for bandgap tuning/engineering, which could be useful for device applications. Thus, ZnO doping with Cd theoretically permits bandgap narrowing and wavelength tunability to blue or even green light spectral range [18]. TiO_2 is also utilized as a Ti source owing to its advantages such as ease, lack of harmfulness, and chemical stability. As an *n*-type semiconductor with a wide energy bandgap, titanium dioxide is well known for its potential applications in the field of photocatalysis, photoelectrochemistry, and optoelectronics because of its excellent optical transmittance and high refractive index. Ti could improve the smoothness of the course of action of the Zn, Cd, and O particles in the appropriate locales into the grid structure, and the Ti-doped samples were methodically controlled for a good-quality nanostructure. For this reason, Ti-doped ZnCdO nanocomposites demand potential applications in the fabrication of optoelectronic and display devices. In the present work, a simple solution method is used for the synthesis of ZnCdO nanocomposites. This method offers a few preferences. For example, minimal effort, simple procedure, and hardware, prepared at room temperature, have enormous scope for the creation of nanostructures, films, and nanopowders, because it is a low-temperature process and it is easy to control the particle size. The main objective of the present study is to prepare the nanocomposites using a simple and cost-effective method. The prepared samples can be used extensively for obtaining novel materials with different properties because, through this process, nano-sized grain particles have been deposited with high purity. The prepared nanocomposites can be utilized in many applications such as luminescence, optoelectronic, and display devices.

Experimental. In the present investigation, chemical compounds such as titanium dioxide (TiO_2), zinc nitrate ($Zn(NO_3)_2$), cadmium nitrate $Cd(NO_3)$, methanol (CH_3OH), and NaOH were purchased from Sigma Aldrich, India. ZnCdO solution was prepared at room temperature by dissolving the appropriate amounts of $Zn(NO_3)_2$ and $Cd(NO_3)_2$ in the presence of NaOH and CH_3OH. In the preparation, 100 mL of 0.1M NaOH was added to the solution of 20 mL containing $Zn(NO_3)_2$ and $Cd(NO_3)_2$ in CH_3OH. After that, 0.01% $Ti(NO_3)_2$ was added, then the solution was stirred for 30 min. Further, a mixture of water to methanol in the ratio of 0.04 was added to the above solution and stirred continuously for up to 30 min. The obtained solution was kept under refrigeration for 2 h, for centrifugation. After the formation of precipitate, it was washed with distilled water several times and then dried at room temperature for more than 24 h, and finally it was calcinated at 450 and 650°C for 2 h by heating at a rate of 15° per minute [19].

X-ray diffraction (XRD) patterns of the samples were taken from the Bruker X-ray diffractometer with a scan rate of 20° per minute using CuK_α radiation. For the prepared samples of pure ZnCdO and nanocom-

posites of Ti-doped ZnCdO, the surface morphology and energy-dispersive X-ray analysis (EDX) were done using Carl Zeiss, Neon 40 Crossbeam, Germany. Photoluminescence (PL) studies were recorded using a 450-W Light Xenon Source on a JobinYvonFluorimeter-FL3-11 spectro-fluorometer.

Results and discussion. *XRD analysis.* XRD patterns of the samples of pure ZnCdO and Ti-doped ZnCdO nanocomposites were shown in Fig. 1. The diffraction angles of 2θ that appeared at 33.1, 38.4, 55.4, 66.8, 82.1, 92.8, and 96.5° indicate (100), (002), (101), (220), (311), and (222) reflections, respectively. The pure and Ti-doped ZnCdO has a face-centered cubic structure because of stronger intensity peaks at 33.1, 38.4, 55.4, and 66.8° corresponding to the 2θ values. Owing to Ti doping, the intensities of the peaks are changed. The zinc oxide has a hexagonal structure corresponding to different planes (100), (002), (101), (102), and (110) with the JCPDS Card no. 89-1397 [20]. The samples of nanocomposites are observed with good intensity as the dopant concentration increases [21, 22]. It shows that Ti could improve the smoothness of the course of action of the Zn, Cd, and O particles in the appropriate locales into the grid structure and the Ti-doped samples were methodically controlled for a good-quality nanostructure. The peak appearing at 25.5° represents a TiO_2 nanoparticle-significant anatase phase with JCPDS Card no. 21-1272 [23]. Another peak that is observed at the diffraction angle 2θ of 49.87° corresponds to ZnCdO [24]. Using Scherrer's equation, the full width at half maximum (FWHM) and the crystalline size of the samples can be calculated with the help of X-ray diffraction pattern [25]:

$$D = \frac{0.9\,\lambda}{\beta\cos\theta}. \qquad (1)$$

The XRD peak value of FWHM is represented by β, and θ is the diffracting angle.

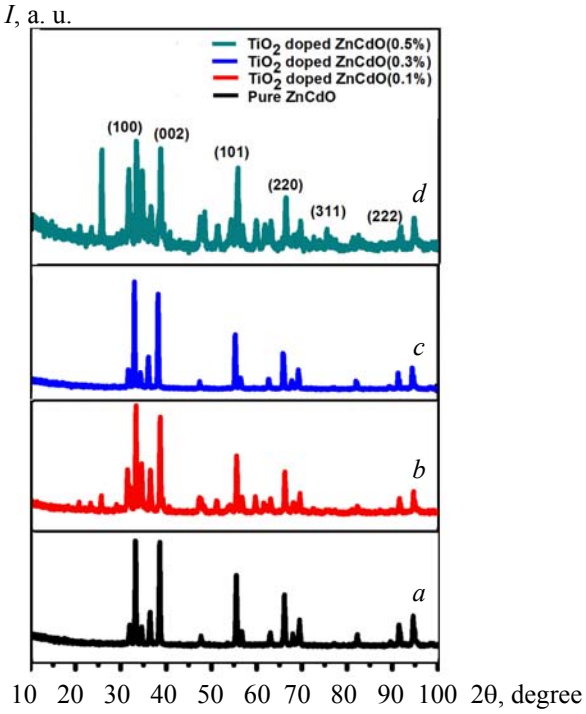

Fig. 1. XRD patterns of (a) pure ZnCdO, Ti-doped ZnCdO for (b) 0.1, (c) 0.3, and (d) 0.5%.

SEM analysis. Figure 2a represents the formation of the irregular grains and morphological features of the prepared samples of pure ZnCdO. The SEM images of pure ZnCdO and nanocomposites of Ti-doped ZnCdO in various wt% (0.1, 0.3, and 0.5%) were observed through the micrographs of Figs. 2b–d. It can be see that the Ti-doped ZnCdO nanocomposites form spherical chunks due to agglomeration. It is suggested that this microstructural transformation could be attributed to the extremely small dimensions of the nanoparticles with high surface energy. From the EDX analysis, the elemental and chemical composition are estimated and presented in Fig. 2. As the agglomeration increases, the number of nanoparticles is also increased. The sample content of ZnCdO characteristic peaks represents confirmation of the occurrences of

Cd, Zn, Ti, and O. Owing to the presence of Ti, the particle size is decreased. From the EDX data, the nanocomposite samples represent the percentage decrement in the Ti-doped ZnCdO.

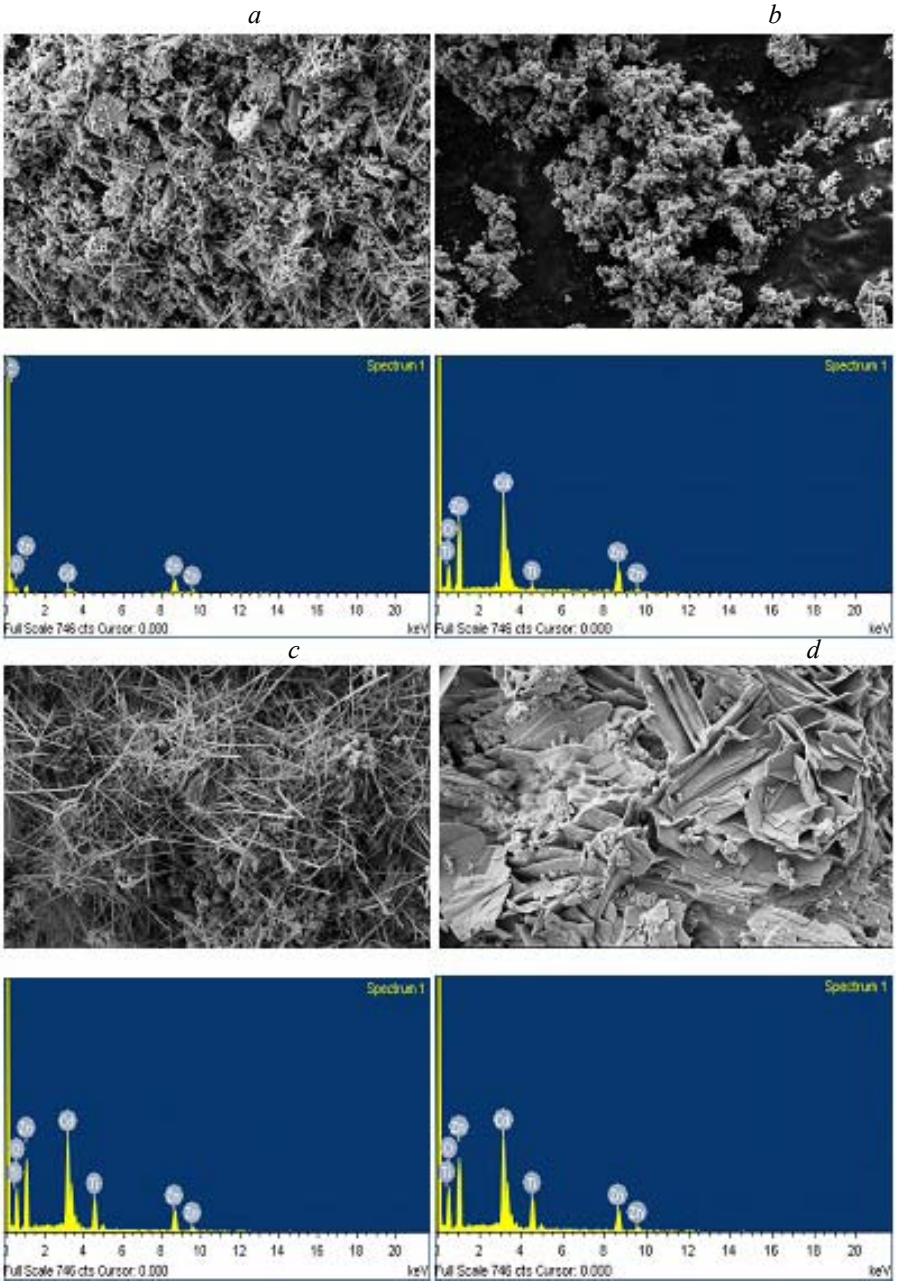

Fig. 2. SEM and EDX images of (a) pure ZnCdO, Ti-doped ZnCdO for (b) 0.1, (c) 0.3, and (d) 0.5%.

W-H graph. Figure 3 shows that the graph, which is plotted 4 sinθ against β cosθ, forms a straight line. It is equal to its slope, which represents the micro strain behavior of the ZnCdO phase. The y-intercept of the prepared samples are found to be 0.00234, 0.00262, 0.00292, and 0.00300 and the particle size of pure ZnCdO is 62.08 nm, whereas Ti-doped ZnCdO (0.1, 0.3, and 0.5%) are found to be 55.05, 50.03, and 45.08 nm. The particle size of the samples shows a decrement in size, as on increasing the Ti concentration [26, 27]. The relation between the crystallite size and dislocation density is represented by [28–31]:

$$\delta = 1 / D^2 , \qquad (2)$$

where D is the crystallite size and δ, the dislocation density.

The obtained values of the crystallite size of the samples are in good agreement with XRD data.

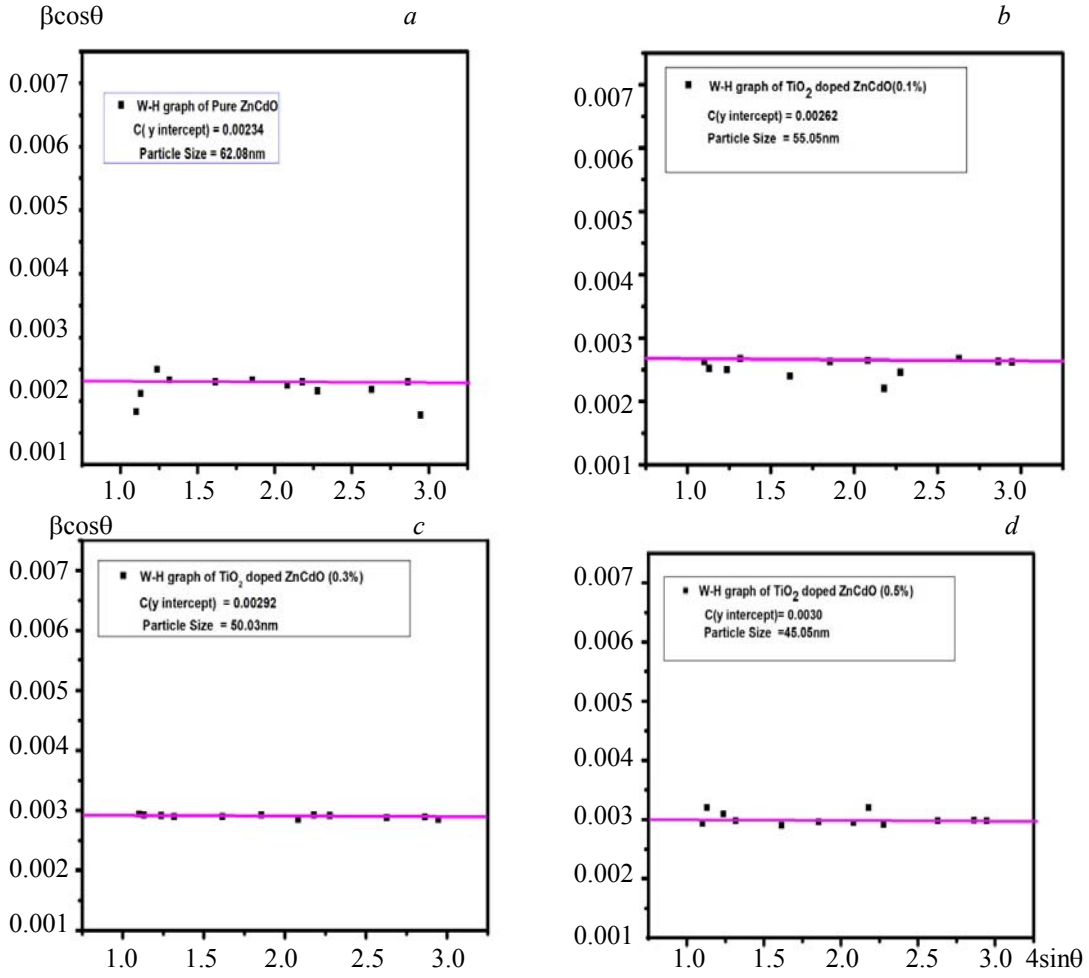

Fig. 3. W-H analysis of (a) pure ZnCdO, Ti-doped ZnCdO for (b) 0.1, (c) 0.3, and (d) 0.5%.

Photoluminescence studies. Photoluminescence spectra give information about excitation and emission wavelength corresponding to the intensity of the emitted radiation. The intensity of the light is plotted against the wavelength on the spectrum. Figure 4 shows the recordings of pure ZnCdO and Ti-doped ZnCdO at room temperature. From the PL spectra, two peaks are observed. The peak observed at 340 nm is due to the contamination present in the synthesized samples. The peak that appeared at 475 nm is due to the direct recombination of conduction electron in the conduction band (Cd) in 3*d* state and a hole in the valance band (O) 2*p* state corresponds to blue emission [32]. The peak observed at 520 nm corresponds to Ti-doped CdO and could be ascribed to the near-band-edge emission [33]. The other peak at 650 nm detected in the visible region indicates the presence of point defects within the bandgap such as vacancies and interstitials known as deep-level emission (DLE) [34, 35]. DLE enhancement can be seen after Ti doping.

The photo-generated electrons have been trapped into Ti^{4+} in the forbidden gap, which enhanced the DLE. Ti^{4+} that occupied Cd^{2+} and Zn^{2+} sites in the lattice structure can trap the electrons that come back from the conduction band to the valence band. The deep level intensity was increased in Ti-doped ZnCdO compared with pure ZnCdO. This referred to an increase in Ti concentration that has been trapped into Ti^{4+} levels in the forbidden gap and then increased the captured electrons within, which as a result enhanced the deep level intensity [36].

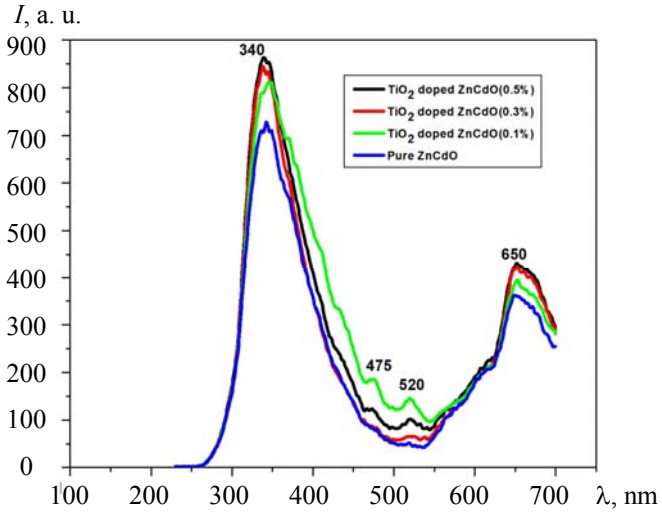

Fig. 4. PL spectra of pure ZnCdO, Ti-doped ZnCdO for 0.1, 0.3, and 0.5%.

Conclusions. Pure ZnCdO and Ti-doped ZnCdO nanocomposites were prepared using a simple solution technique. From the XRD patterns, the prepared nanocomposite was within the nanoscale range. The presence of ZnCdO forms spherical chunks with irregular grains due to agglomeration. The particle size of the pure ZnCdO was found to be 62.08 nm, whereas Ti-doped ZnCdO (0.1, 0.3, and 0.5%) were 55.05 and 50.03, and 45.05 nm. The peak that appeared at 475 nm is due to the direct recombination of a conduction electron in the conduction band (Cd) in 3*d* state and a hole in the valance band (O) 2*p* state corresponds to blue emission. The peak observed at 520 nm corresponding to Ti-doped CdO could be ascribed to the near-band-edge emission. The other peak at 650 nm detected in the visible region indicates the presence of point defects within the bandgap such as vacancies and interstitials known as DLE. The photo-generated electrons have been trapped into Ti^{4+} in the forbidden gap, which enhanced the deep level emission. Ti^{4+} that occupied Cd^{2+} and Zn^{2+} sites in the lattice structure can trap the electrons that come back from the conduction band to the valence band. The expected outcomes of the present work are suitable for the development of display devices and optoelectronic gadget applications.

REFERENCES

1. P. H. Jefferson, S. A. Hatfield, T. D. Veal, P. D. C. King, C. F. McConnville, J. Z. Perez, V. M. Sanjose, *Appl. Phys. Lett.*, **92**, 022101 (2008).
2. R. K. Chava, M. Kang, *J. Alloys Compd.*, **692**, 67–76 (2017).
3. S. A. Bidier, M. R. Hashim, A. M. Al-Diabat, M. Bououdina, *Phys. E*, **88**, 169–171 (2017).
4. R. Mechiakh, R. Bensaha, *Cond. Mater.*, **7**, 54–57 (2006).
5. W. Yu, T. Liu, S. Cao, C. Wang, C. Chen, *J. Solid State Chem.*, **239**, 131–138 (2016).
6. R. C. Weast, S. M. Selby, In: *Chemistry and Physics in CRC*, 3rd ed., Taylor and Francis (1976).
7. E. K. Abdul-Hussein, A. M. Hayder, A. I. Khudiar, *J. Mater. Res. Tech.*, **2**, No. 2, 182–187 (2013).
8. T. Ahmad, S. Khatoon, K. Coolahan, S. E. Lofland, *J. Mater. Res.*, **28**, 1245–1253 (2013).
9. Y. Su, F. Peng, Z. Jiang, *Biomaterials*, **32**, 5855–5862 (2011).
10. Z. Han, J. Zhang, X. Yang, W. Cao, *Solar Energy Mater. Solar Cells*, **95**, 483–490 (2011).
11. M. Taukeer Khan, R. Bhargav, A. Kaur, et al., *Thin Solid Films*, **519**, No. 3, 1007–1011 (2010).
12. S. Ashoka, G. Nagaraju, K. V. Thipperudraiah, et al., *Mater. Res. Bull.*, **45**, No. 11, 1736–1740 (2010).
13. M. Liu, Y. Du, L. Ma, et al., *Int. J. Hydrogen Energy*, **37**, No. 1, 730–736 (2012).
14. X. L. Yang, J. Zhang, S.-B. Ren et al., *Inorg. Chem. Commun.*, **13**, No. 1, 1337–1339 (2010).
15. M. H. Vijaykumar, P. A. Vaishampayan, Y. S. Shouche, T. B. Karegoudar, *Enzym Microbiol. Tech.*, **40**, No. 2, 204–211 (2007).
16. S. Balachandran, S. G. Praveen, R. Velmurugan, M. Swaminathan, *RSC Adv.*, **4**, 4353–4362 (2014).
17. T. O. Mahony, E. Guibal, J. M. Tobin, *Enzym Microbiol. Tech.*, **31**, 456–463 (2002).

18. T. Makino, Y. Segawa, M. Kawasaki, A. Ohtomo, R. Shiroki, K. Tamura, T. Yasuda, H. Koinuma, *Appl. Phys. Lett*., **78**, 1237 (2001).
19. D. V. Sathish, Ch. Rama Krishna, Ch. Venkata Reddy, T. Raghavendra Rao, P. S. Rao, R. V. S. S. N. Ravikumar, *J. Mol. Struct*., **1034**, 57–61 (2013).
20. A. M. Ismail, A. A. Menazea, H. A. Kabary, A. E. El-Sherbiny, A. Samy, *J. Mol. Struct*., **1196**, 332–327 (2019).
21. P. Shokeen, A. Jain, A. Kapoor, *Opt. Mater*., **67**, 32–37 (2017).
22. K. Qi, B. Cheng, J. Yu, W. Ho, *J. Alloys Compd*., **727**, 792–820 (2017).
23. G. Li, X. Wang, Y. Wang, X. Shi, N. Yao, B. Zhang, *Phys. E*, **40**, 2649 (2008).
24. D. V. Sathish, Ch. Rama Krishna, Ch. Venkata Reddy, U. S. Udayachandran Thampy, R. V. S. S. N. Ravikumar, *Phys. Scr*., **86**, 035708 (2012).
25. A. Wang, J. R. Babcock, N. L. Edleman, A. W. Metz, M. A. Lane, R. Asahi, V. P. Dravid, C. R. Kannewurf, *PNAS*, **98**, 7113–7116 (2001).
26. M. Yuste, R. E. Galindo, O. M. Sacristan, I. Minguez-Bacho, R. Sonia, M. Hernandez-Velez, O. Sanchez, *Mater. Res. Express*, **1**, 045028 (2014).
27. W. Zhang, J. Zhao, Z. Liu, Z. Liu, *Appl. Surf. Sci*., **284**, 49–52 (2013).
28. Z. R. Khan, M. Zulfequar, M. S. Khan, *Mater. Sci. Eng. B*, **174**, 145–149 (2010).
29. P. Rajeswari, S. Dhanuskodi, *Cryst. Res. Technol*., **48**, 589–598 (2013).
30. V. Radhika, V. Annamalai, G. Vijaya, D. Annakkodi, *J. Environ. Nanotechnol*., **5**, No. 3, 39–43 (2016).
31. E. F. Abo Zeida, I. A. Ibrahem, A. M. Ali, W. A. A. Mohamed, *Res. Phys*., **12**, 562–570 (2019).
32. S. Balamurugan A.R. Balu K. Usharani M. Suganya, S. Anitha, D. Prabha, S. Ilangovan, *Pacific Sci. Rev. A: Nat. Sci. Eng*., **18**, No. 3, 228–232 (2016).
33. Kuo Tz-Jun, Michael H. Huang, *J. Phys. Chem. B*, **110**, 13717–13721 (2006).
34. T. Akilan, N. Srinivasan, R. Saravanan, *Mater. Sci. Semicond. Proc*., **30**, 381–387 (2015).
35. B. Panigrahy, M. Aslam, D. S. Misra, M. Ghosh, D. Bahadur, *Adv. Funct. Mater*., **20**, No. 7, 1161–1165 (2010).
36. S. A. Bidier, M. R. Hashim, M. Bououdina, *J. Mater. Sci. Mater. Electron*., **28**, 11178–11185 (2017).